A Systematic ANSI S1.11 Filter Bank Specification Relaxation and Its Efficient Multirate Architecture for Hearing-Aid Systems

Cheng-Yen Yang, Chih-Wei Liu, *Member, IEEE*, and Shyh-Jye Jou, *Senior Member, IEEE*

***Abstract*—Recently, emerging mobile computing requires the high integration of hearing aids into a single system-on-chip. Modern hearing aid systems include a frequency decomposer, noise reduction, feedback cancellation, auditory compensation, and intelligent adaptation. The majority of existing works concentrated on improving the performance and efficiency on a single-signal processing block or one-sided effect. These works lacked comprehensive discussions on system-wide aspects regarding the overall impacts. To design an optimal hearing aid system, frequency decomposers, or the filter banks that dominate in hearing aid systems, are the first priority. We propose a systematic relaxation of the ANSI S1.11 specification and its design procedure for filter banks. The proposed design procedure overcomes the drawbacks of previous works and changes the five performance indices of the filter bank: delay, complexity, sub-band rate reduction, ripples of synthesized output, and prescription matching errors. These performance indices help system or algorithm designers in selecting a beneficial system-relaxed filter bank to achieve optimal hearing aids. The proposed multirate filter bank using the resampling method provides an efficient, low complexity, and delay-constrained computing architecture. Finally, seven design cases are used to demonstrate the proposed method, and comprehensive discussions of the five performance indices are presented.**

***Index Terms*—ANSI S1.11, hearing aids, multirate filter bank, NAL-NL1, prescription matching, quasi-ANSI.**

I. Introduction

In modern hearing aids, the analysis filter banks play a crucial role and have a significant influence on the entire hearing aid system [1], which mainly involves auditory compensation, noise reduction, and feedback cancellation. The design considerations of a filter bank for hearing aids involve not only the computation complexity but also the latency, frequency resolution, prescription matching capability, interactive influence on noise reduction algorithms, and the intelligibility and quality of speech. Many of these considerations are influenced by positive or negative effects with each other.

One important issue regarding the filter bank design for use in hearing aids is the tradeoff among frequency resolution, complexity, and phase distortion. To provide sufficiently fine frequency resolution while significantly reducing the complexity, the frequency warping technique has been applied to filter banks [1], cosine-modulated filter banks [2], and FFTs [3]. The main idea is to cascade all-pass filters in their prefilters or delay lines to alter the time interval of samples, which transforms a uniform frequency distribution into a non-uniform distribution with a shorter filter length or smaller point size. Moreover, the frequency warping approach provides a high degree of frequency resolution alteration for the filter bank and a better match to the psychoacoustic model [4]. Regarding implementation, the frequency warping approach can be adopted to design an efficient frequency decomposer using a reconfigurable architecture [5]. The recent study of a warped cosine-modulated filter bank in [2] has revealed an efficient low complexity result. However, the major side-effect of frequency warping is that the non-linear phase property of the cascaded all-pass filters introduces severe frequency-dependent phase distortion. In Kate's early work [3] on using frequency warping in FFT-based hearing aids, the experimental results indicated that the phase distortion phenomenon induced by frequency warping both annoyed normal-hearing and hearing-impaired persons.

In fact, the phase distortion of the filter bank might not be allowable for modern digital hearing aids because the acoustic signal processing followed by the analysis filter bank are highly reliant on the cues hidden in the sub-band signals. The phase distortion could generate inharmonicity to the periodic signals and misalignment in time [6]. For the monaural hearing aid digital signal processing (DSP) algorithm, the glottal feature extraction or the estimation of fundamental frequency would be incorrect due to the inharmonicity. Furthermore, the phase information is crucial for the binaural hearing aid DSP algorithm [1], [7], which can accurately localize sound sources. According to headphone experiments in [8], listeners can distinguish two sound sources in an azimuth of 1–5°, corresponding to 10–15 us interaural time differences. For an example of a 24 kHz sampling rate hearing aid, only a few phase-distorted samples would deteriorate the performance of the binaural hearing-aid DSP algorithm. Furthermore, the cost of perfect phase compensation for the IIR analysis filter bank is extremely high [3] compared to that of the (linear-phase) finite-impulse response (FIR) one. Therefore, linear-phase FIRs are the only option for hearing aid implementation. If complexity/delay needs to be lower under the linear-phase condition of filter banks, the frequency resolution should be wider. In other words, a relaxed filter specification is required.

Manuscript received September 29, 2015; revised February 6, 2016 and April 16, 2016; accepted April 17, 2016. Date of publication April 20, 2016; date of current version May 27, 2016. The associate editor coordinating the reviewof this manuscript and approving it for publication was Prof. Bozena Kostek.

The authors are with the Department of Electronics Engineering, National Chiao Tung University, Hsinchu 300, Taiwan (e-mail: chenyen.yang@gmail.com; cwliu@twins.ee.nctu.edu.tw; jerryjou@mail.nctu.edu.tw).

Color versions of one or more of the figures in this paper are available online at http://ieeexplore.ieee.org.

Digital Object Identifier 10.1109/TASLP.2016.2556422

The ANSI S1.11 specification [9] has been widely used in acoustic spectrum analyzers and adopted by some well-known prescription algorithms for hearing aids, such as NAL-NL1 [10] and Aescu HRL-1 [11] for Mandarin. This type of octave band filter bank can mimic the psychoacoustic model well, but the overall delay was considered to be no longer than 10–20 ms [12], [13]. To overcome this long delay equipped by the standard ANSI S1.11 filter bank, e.g., 78 ms in [14], Liu *et al.* [15] have proposed a specification relaxation method by parametric expansion of some sub-filters to meet the latency constraint of 10 ms. This quasi-ANSI filter bank [15] applied a straightforward approach and thereby lacked some systematic investigations, and thus, it might not be the optimal ANSI specification relaxation. For example, the possible expanded pass-band coverage range and the allowable inter-band interference can affect the prescription matching capability. A previous study [7] has revealed that the increase in the pass-band coverage would degrade the speech intelligibility and make prescription matching difficult.

To design an optimized low-delay filter bank for modern hearing aids, we propose a method for the systematic relaxation of the ANSI S1.11 specification and the design procedures. By using the proposed design procedures, the relaxed system-relaxed ANSI filter banks do not require as many time-consuming trials as previously because the early performance estimation during the early design stage helps the final result coincide with the expected design goals. The specification relaxation occurs when one of the performance indices, such as delay or complexity, violates the given constraints. The relaxed parameters are not only applied on the individual sub-filter but also accordingly control and investigate the minimum and maximum attenuation constrains of the ANSI S1.11 specification. Consequently, keeping the octave band property, the system-relaxed parameters control the overlapping factor of successive sub-filters. The systematic relaxed ANSI filter bank can shrink the specification parameters to guarantee the prescription matching capability. When filter banks are designed, their prescription matching capabilities are characterized as interband aliasing of sub-filters or the average matching errors among a group of patients. This will be the criterion for determining whether the design qualifies for different degrees and types of hearing-loss. In addition, to minimize the sound quality degradation by filter banks, the ripples of the summed output should be lower and within tolerable ranges after gain equalization.

Previous studies [14], [16], [17] primarily focused on the low complexity design of the analysis filter bank for hearing aids. They did not consider the involved computation of the sub-band signal processing followed by the analysis filter bank, for example, the monaural or binaural noise reduction algorithm and the wide dynamic range compression (WDRC). Efficiently downsampling the rate of the sub-band signal toward its Nyquist rate can significantly reduce the system complexity [18]. Nevertheless, a rational sampling rate converter (SRC) is necessary, which considerably increases the complexity. By applying the elegant polyphase decomposition [19], this paper proposes an efficient multirate architecture for the system-relaxed Nyquist ANSI filter bank. The proposed system-relaxed Nyquist ANSI filter bank saves approximately 11% of computation complexity compared to that of the quasi-ANSI filter bank [15], while achieving a better prescription matching capability. Moreover, to further decrease the sampling rate of each sub-band signal, approximately 13.4% of the computational complexity of the noise reduction algorithms and WDRC, followed by the systematic relaxed Nyquist ANSI filter bank, will be saved.

Finally, this systematic approach combines implementation issues (delay, complexity, and sub-band rate reduction), prescription matching (matching errors/interband aliasing), and sound quality (ripples of summed output) to guide hearing aid designers in designing a beneficial filter bank for hearing aid systems. The remainder of this paper is organized as follows. Section II briefly introduces the standard class-2 ANSI S1.11 filters. By investigating and controlling the minimum and maximum attenuation constrains of the ANSI filter, the proposed system relaxation of the ANSI S1.11 specification will be presented. In Section III, we exploit an efficient multirate filtering architecture by the re-sampling method to implement the proposed system-relaxed Nyquist ANSI filter bank. Some design examples with different constraints are described in Section IV to demonstrate the success of the proposed systematic relaxation approach and its design procedure. Finally, Section V concludes this paper.

II. ANSI S1.11 Standard and The Proposed Specification Relaxation Method

The ANSI S1.11 specification [9] defines several mathematical rules on the limit or the minimum and maximum attenuations, called the relative attenuations, for class-0, class-1, and class-2 octave-band and fractional octave-band filters. In this paper, we choose the class-2 specification to avoid the long delay problem, and its stop-band attention (60 dB) is sufficient for most of the degrees of hearing loss. By satisfying these relative attenuations, one could obtain a filter bank that meets the requirements of the ANSI S1.11 specification. For readers' reference, a brief introduction to the standard ANSI S1.11 fractional-octave class-2 filters is provided in the following section. For further details, please refer to [9].

A. ANSI S1.11 Specification

The fractional octave-band sub-filters can be obtained by dividing the octave band with a bandwidth designator, denoted by b. For example, for the 1/3-octave filter band, $b = 3$. The mid-band (or central) frequency $f_c(n)$ of the nth fractional-octave sub-filter is defined as

$$f_c(n) = 2^{\frac{1}{b}} f_c(n-1). \tag{1}$$

Fig. 1 depicts the relative attenuation regulation of the class-2 nth fractional-octave sub-filter, in which there are a total of 19 break points [solid dots: 7 in Fig. 1(a) and 12 in Fig. 1(b)], defining the minimum and maximum attenuation limits. The normalized frequency axis Ω_n for each sub-filter with respect to its mid-band frequency is defined by $\Omega_n = f/f_c(n)$, where f is the original frequency. Then, the relative attenuation of the class-2 nth sub-filter shown in Fig. 1 can be directly applied to other sub-filters. The allowed ripple in the passband is ± 0.5 dB,

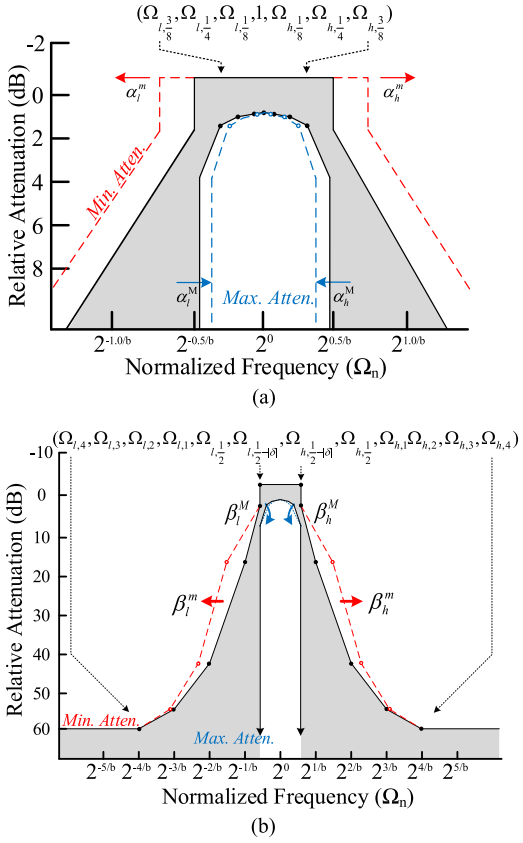

Fig. 1. Limits on relative attenuation for the class-2 octave band specification. The black solid line represents the original limits of ANSI S1.11, and the colored dashed line is the proposed relaxation of the specification. (a) Bandwidth relaxation and (b) transition relaxation.

and the stopband attenuation should be larger than 60 dB. For fractional-octave sub-filters, the frequency scale needs to be linearly transformed with respect to the band edge frequencies. Therefore, the high- and low-frequency sides of the break points, denoted by $\Omega_{h,i}$ and $\Omega_{l,i}$, respectively, for the class-2 fractional octave band will be calculated by

$$\Omega_{h,i} = 1 + \frac{(2^{1/2b} - 1)}{(2^{1/2} - 1)}(\Omega - 1), \text{ and } \Omega_{l,i} = \frac{1}{\Omega_{h,i}}, \qquad (2)$$

where $\Omega = 2^i$, $i = \frac{1}{8}$, $\frac{1}{4}$, $\frac{3}{8}$, $\frac{1}{2} - |\delta|$, $\frac{1}{2}$, 1, 2, 3, and 4, with a very small value of δ, i.e., $\delta \to 0$. Note that another break point is located on mid-band frequency $(i = 0)$ such that the overall 19 break points are well defined. Then, referring to the class-2 specification, the minimum attenuation on the high-frequency side is determined by the break points $\Omega_{h,i} = (\Omega_{h,\frac{1}{2}-|\delta|}, \Omega_{h,\frac{1}{2}}, \Omega_{h,1}, \Omega_{h,2}, \Omega_{h,3}, \Omega_{h,4})$, and the corresponding attenuations are $(-0.5, 1.6, 16.5, 41, 55, 60)$ in decibels. The maximum attenuation on the high-frequency side is mostly defined in Fig. 1(a) by the break points $\Omega_{h,i} = (1, \Omega_{h,\frac{1}{8}}, \Omega_{h,\frac{1}{4}}, \Omega_{h,\frac{3}{8}}, \Omega_{h,\frac{1}{2}-|\delta|}, \Omega_{h,\frac{1}{2}})$, and the attenuation values are $(0.5, 0.6, 0.8, 1.6, 5.5, 5.5)$ in decibels. Both frequency sides are symmetrical in the logarithmic scale, and thus, the low-frequency part can be obtained by $\Omega_{l,i} = \frac{1}{\Omega_{h,i}}$. Then, the band-edge low and high frequencies, denoted by $f_l(n)$ and $f_h(n)$, of the nth sub-filter are determined by

$$f_l(n) = \Omega_{l,\frac{1}{2}} \times f_c(n) \text{ and } f_h(n) = \Omega_{h,\frac{1}{2}} \times f_c(n). \qquad (3)$$

The bandwidth of the nth sub-band, i.e., $BW(n)$, is

$$BW(n) = f_h(n) - f_l(n). \qquad (4)$$

According to the requirements of our hearing aid system, the pass-band frequencies of the filter bank should be covered from 125 Hz to 10 kHz, which covers most of the fundamental frequencies for humans [20]. Moreover, the 1/3-octave specification is chosen in the same way as the prescription algorithm used. Therefore, b is set as 3 and n is considered to range from 22 to 39. We have six octave bands with a total of 18 sub-filters, denoted by $F_{22} \sim F_{39}$, and the mid-band frequency of F_{22} is 157 Hz. With the selected 18 sub-filters, the sampling rate of the input signal will be set to 24 kHz [14].

B. Proposed ANSI S1.11 Specification Relaxation

The tight filter specification of some sub-filters, such as $F_{22} \sim F_{24}$, makes the ANSI 1/3-octave filter bank complicated and results in a rather long delay [14], which is greater than 20 ms. To address this issue, Liu *et al.* [15] have developed a parametric bandwidth expansion for individual sub-filters subjected to the delay of each sub-filter within the quasi-ANSI filter bank $\leq$10 ms. The specification relaxation applied in the quasi-ANSI filter bank [15] is a straightforward approach and thus requires many trials for designing an individual sub-filter. The determined design constraints might vary in different initial conditions for different filters. The designer cannot predict the performance of the quasi-ANSI filter bank prior to completing the design of all filters. Consequently, one cannot determine the optimized relaxation parameters during the early design stage. Furthermore, the possible expanded pass-band coverage range and the allowable inter-band interference would affect the prescription matching capability of the filter bank. Fig. 1 shows the proposed systematic relaxation of the ANSI S1.11 specification. Rather than determining the relaxed design specification for an individual filter, the proposed systematic relaxation approach determines the new locations of break points at band edge frequencies, and hence, both the minimum and maximum attenuations are changed.

The system-relaxed algorithm first defines the following α-series parameters, which control the bandwidth expansion of the minimum attenuation, i.e., (α_h^m, α_l^m), and the contraction of maximum attenuation, i.e., (α_h^M, α_l^M), as shown in the upper part of Fig. 1(a). The new location of the break points at band edge frequencies can be calculated by

$$\Omega^m_{h,\frac{1}{2}} = \Omega_{h,\frac{1}{2}} \times (1 + \alpha_h^m), \qquad (5)$$

and

$$\Omega^m_{l,\frac{1}{2}} = \Omega_{l,\frac{1}{2}} \times (1 - \alpha_l^m). \qquad (6)$$

Note that the offset between the new and old locations of the break points can be obtained by

$$\Delta\Omega_h^m = \Omega_{h,\frac{1}{2}} \times \alpha_h^m, \qquad (7)$$

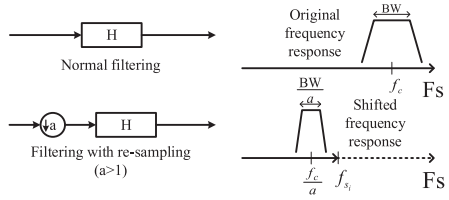

Fig. 2. Effect of sampling rate alteration.

and

$$\Delta\Omega_l^m = \Omega_{l,\frac{1}{2}} \times \alpha_l^m . \tag{8}$$

Second, the algorithm defines the β-series parameters that change the locations of the break points (horizontal shift), which result in changes of the slopes of the relative attenuation lines in the passband-to-stopband transition of minimum attenuation (β_h^m, β_l^m) and passband of maximum attenuation (β_h^M, β_l^M), as shown in Fig. 1(b). The new locations of the break points corresponding to these parameters can be determined by

$$\Omega_{h,i}^m = \Omega_{h,i} \times (1 + \beta_h^m) + \Delta\Omega_h^m \tag{9}$$

and

$$\Omega_{l,i}^m = \Omega_{l,i} \times (1 - \beta_l^m) - \Delta\Omega_l^m , \tag{10}$$

where $i = 1$, 2, 3, and 4. The extra offsets $\Delta\Omega_h^m$ and $\Delta\Omega_l^m$ in (9) and (10) are contributed by the passband relaxation in (5) and (6), respectively. Additionally, note that the relaxations on maximum attenuation (α_h^M, α_l^M, β_h^M, and β_l^M) are neglected because they do not contribute significant effects. However, one can still adopt a similar approach with equations (5) to (10) to perform the relaxation on the maximum attenuation, if necessary.

III. Proposed Efficient Multirate Architecture for ANSI-Like S1.11 Filter Banks

The concept of re-sampling for FIR filters is that decreasing/increasing the sampling rate of the filter's input can result in the frequency shifting left/right and the (magnitude) response of the FIR filter contracting/expanding without any phase distortion. Fig. 2 illustrates the effect of altering the filter's sampling rate. If the input is decimated by a factor of a, $a > 1$, in the time domain, then it will cause a left shift and contraction of the filter response by a factor of $1/a$ in the frequency domain.

As shown by equations (1)–(4), for an ANSI-like filter bank, sub-filter F_n can be considered to be the version of sub-filter F_{n+1} contracted by a factor of $2^{\frac{1}{3}}$, similar to Fig. 2. In other words, one can apply the sampling rate alteration method to obtain F_n by decimating F_{n+1} by a factor of $1/2^{\frac{1}{3}}$. By repeating a similar method to design the other sub-filters, an efficient multirate architecture for an ANSI-like FIR filter bank can then be developed by applying H_{39} (sub-filter belonging to sub-band F_{39}) as the prototype filter (see Fig. 3). Note that the proposed architecture for an ANSI-like filter bank requires various SRCs. The downsampling factor within each SRC is obtained by selecting the adequate fraction or integer close to the reciprocal of the normalized lowest sampling rate of the sub-filter, i.e., its normalized Nyquist rate. For example, to design F_{35}, a SRC

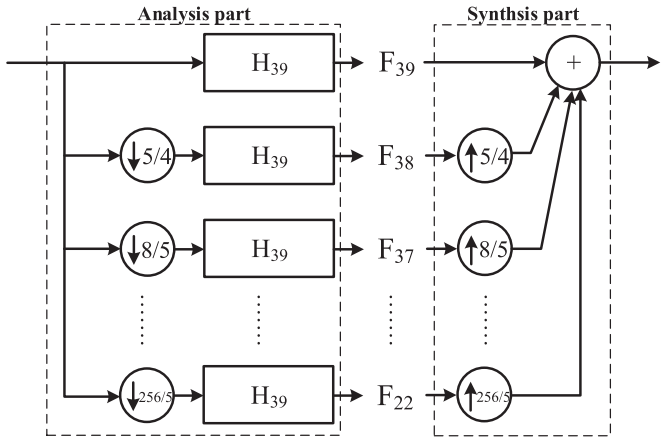

Fig. 3. Demonstration of re-sampling method using H_{39}.

TABLE I
Nyquist Rate of Each Sub-Band Signal of Quasi-ANSI 1/3-Octave Band Filter Bank and Selected Factors for Filter Re-Sampling Method

Sub-band F_n	Nyquist Rate (Norm. to Fs) ANSI-S1.11	Practical decimation factors D_n or M_n/L_n			
		ANSI-S1.11	*Yang et al.* [18]	*Liu et al.* [15]	proposed
F_{39}	1.0000	1	1	1	1
F_{38}	0.7937	5/4	5/4	1	5/4
F_{37}	0.6299	8/5	8/5	1	8/5
F_{36}	0.5000	2	2	2	2
F_{35}	0.3968	10/4	(2, 5/4)	2	(2, 5/4)
F_{34}	0.3149	16/5	(2, 8/5)	2	(2, 8/5))
F_{33}	0.2500	4	4	4	4
F_{32}	0.1984	20/4	(4, 5/4)	4	(4, 5/4)
F_{31}	0.1574	32/5	(4, 8/5)	4	(4, 8/5)
F_{30}	0.1250	8	(4, 8/5)	4	4
F_{29}	0.0992	40/4	(4, 8/5)	4	4
F_{28}	0.0787	64/5	(4, 8/5)	4	4
F_{27}	0.0625	16	(4, 8/5)	4	4
F_{26}	0.0496	80/4	(4, 8/5)	4	4
F_{25}	0.0393	128/5	(4, 8/5)	4	4
F_{24}	0.0312	32	(4, 8/5)	4	4
F_{23}	0.0248	160/4	(4, 8/5)	4	4
F_{22}	0.0196	256/5	(4, 8/5)	4	4

with a downsampling factor of $1/2^{4/3} = 0.3968$ is required. We select a decimation factor of $10/4$ (Table I), which is close to the reciprocal of 0.3968.

To prevent the aliasing problem, frequently decimating a filter requires a low-pass filter to suppress possible aliasing distortion [21], which results in an extra processing delay [22]. The delay, i.e., the tap length, of the anti-aliasing filter is dependent on the rate alteration factor, which will considerably increase, e.g., 256/5 in Fig. 3 or Table I. Indeed, an M-fold decimator provides a lower data rate for the filter's processing and can hence decrease the computational complexity. However, increasing M is equivalent to tightening the design constraint of the pre-aliasing filter, which will increase the complexity and the delay. Constrained by the minimized number of MPY/S (multiplications per sample), an optimized decimation factor will exist for designing the sub-filter. From the exploration results in [15], it was

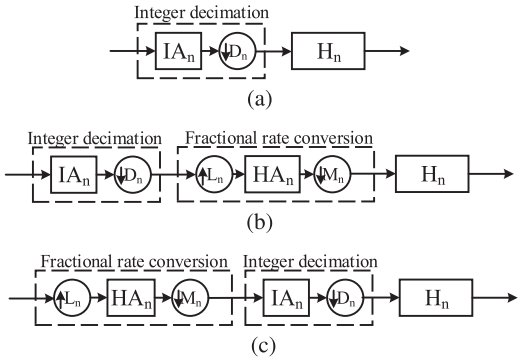

Fig. 4. Architecture exploration for analysis bank: (a) Implementation-aware, (b) complexity-aware and (c) latency-complexity constrained.

concluded that the optimized decimation factor for sub-filter F_{22} lies in the range of $(4, 7)$. In other words, the maximum resampling factor for F_{22} should be less than 7, which contradicts the factor of 256/5 shown in Fig. 3. This fact implies that the architecture in Fig. 3 should be modified to obtain an optimized low-complexity ANSI-like filter bank.

A. Architecture Exploration for Efficient Multirate ANSI-Like S1.11 Filter Bank

Exploiting the sampling rate alteration method to design sub-filter F_n might include an integer decimation factor, denoted by D_n, or a fractional factor M_n/L_n, and/or both for different design considerations. Taking F_{22} as an illustrative example, a factor of 32 was considered in [14] for low cost, a factor of 4 was used in [15] for low delay, and a factor of 4 followed by 8/5, denoted by $(4, 8/5)$-decimator, i.e., a factor of 6.4, was determined in [18] for both low complexity and delay. Fig. 4(a) presents an implementation-aware architecture for designing F_n with an integer factor D_n, where IA_n is the necessary pre-aliasing filter. The detailed design procedures for H_n and the associated IA_n can be found in [14] or [15]. The cost of the folded architecture in [14] is minimized due to the 32-fold decimator; however, it suffered from a rather long delay, i.e., 78 ms. In contrast, for the 10 ms delay constraint, a decimation factor of 4 in [15] or 6.4 in [18], both of which fall in (4,7), was determined. Fig. 4(b) and (c) depict the multirate architecture for designing F_n with both a D_n (i.e., the integer decimation part) and M_n/L_n (i.e., the fractional rate conversion part). To reduce the computational complexity, one would desire the filter to be operated at a lower sampling rate conversion. By placing the integer decimation prior to the fractional rate conversion [see Fig. 4(b)], the complexity-aware multirate architecture is then developed. However, down-sampling is beneficial for keeping the fractional rate conversion operating at a rate that is as low as possible, but the anti-aliasing filter of the fractional rate conversion might contribute an extra (or unacceptable) delay. An alternative design called latency-complexity constrained multirate architecture is considered [see Fig. 4(c)], in which the cascading order of the rate conversion differs from that in Fig. 4(b).

For the readers' reference, the detailed decimation factors used in multiple-stage [18] and single-stage [15] multirate architectures for $F_{22} \sim F_{39}$ are listed in the fourth and fifth columns of Table I. The multiple-stage multirate architecture [18] is superior in both complexity and sub-band sampling rate reduction; however, this superiority comes at the cost of an extra delay contributed by the fractional rate conversions. Similar results can be found in [23]. For the multiple-stage sampling rate conversion in Fig. 4(b) and (c), it is difficult to determine which one is superior. The experimental results in [23] suggested that for the two-stage down-sampling rate conversion, it is better to have a larger decimation factor in the first stage to reduce the computational complexity. This result indicates that a hybrid architecture with a compromise design should be adopted to design the optimized multirate architecture.

Choosing between the architectures in Fig. 4(b) and (c) depends on the applied decimation factors: D_n and M_n/L_n for sub-filter F_n. For the example of the $(D_n = 4, \frac{M_n}{L_n} = \frac{8}{5})$-decimator for F_{32}, it requires two down-sampling rate conversions, i.e., a factor of $D_n = 4$ and of $M_n = 8$. Based on the suggestions of [23], the architecture in Fig. 4(c) is preferred because placing the larger decimation factor in the prior stage is better for reducing the complexity. In contrast, for sharper sub-filters, e.g., $F_{30} \sim F_{22}$, which dominate the principal delay of the filter bank, although the multiple-stage multirate architecture [18] requires less multiplications per sample, the induced fractional $8/5$-decimator would contribute an additional delay. To meet the delay constraint, similar to [15], this paper adopts the implementation-aware architecture for $F_{30} \sim F_{22}$.

The proposed hybrid architecture for an ANSI-like FIR filter bank is shown in Fig. 5, in which the sub-filters $F_{39} \sim F_{31}$ are implemented by the latency-complexity constrained architecture with the prototype filter H_{18}, while the others ($F_{30} \sim F_{22}$) are applied by the implementation-aware architecture using sub-filters $H_9 \sim H_1$. The remaining sub-filters, including HA_i, IA_i, IA_i', IA_i'', IS_i, IS_i', and IS_i'', where $i = 1, 2$, are anti-aliasing filters that are required for rate conversions. Table II summarizes the comparison of the proposed hybrid architecture with that of [15] and [18] for the 18-band quasi-ANSI filter bank. The multiple-stage multirate architecture [18] is superior in terms of both the complexity and the sampling rate reduction performance; however, the delay (i.e., 13.58 ms) is the worst. Although the MPY/S of the proposed hybrid architecture is slightly increased, compared with the single-stage multirate architecture [15], a sampling rate reduction of approximately 13.42% is achieved, which considerably reduces the complexity of the follow-up DSP algorithms. The proposed hybrid architecture is indeed a compromise design for realizing the ANSI-like FIR filter bank.

B. Proposed Design Procedure of the Filter Bank

For the optimized system-relaxed ANSI FIR filter bank for digital hearing aids, Fig. 6 presents the proposed design procedure, which consists of six steps:

1) Define Desired Filter Bank Specification: Initially, the designer should determine the required number of octave bands q and the bandwidth designator b, i.e., a filter bank with $q \times b$ sub-filters to cover the desired frequency range. In addition,

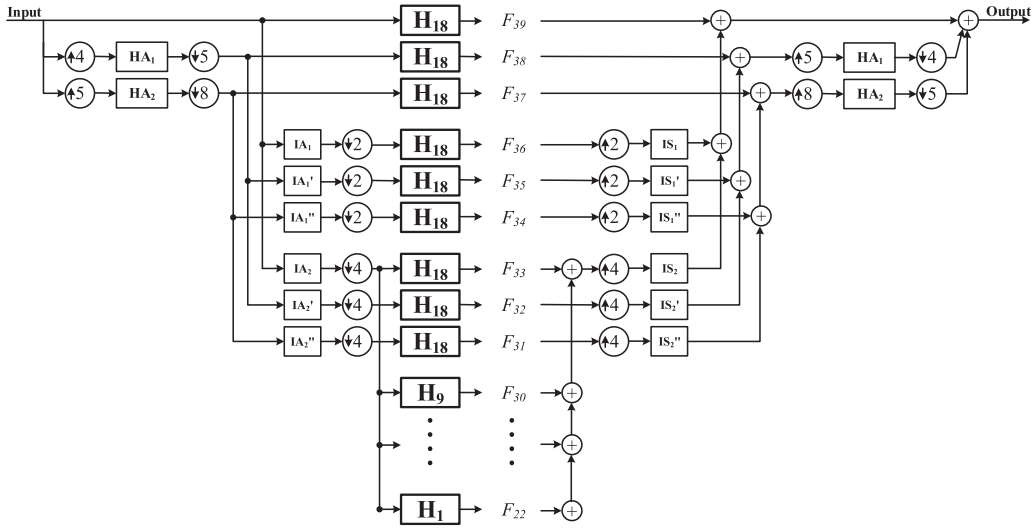

Fig. 5. The proposed filter bank architecture.

TABLE II
EVALUATION OF DIFFERENT MULTIRATE ARCHITECTURES FOR QUASI-ANSI FILTER BANK

Architecture	Complexity (MPY per sample) Rat. conv.	$F_{39} \sim F_{31}$	$F_{30} \sim F_{22}$	Total	Delay (ms)	Sampling rate reduction (%)
[15]	30 (13%)	105 (46%)	91 (40%)	226	10.00	100.00
[18]	91 (47%)	41 (21%)	60 (31%)	192	13.58	75.33
proposed	91 (35%)	105 (41%)	60 (23%)	255	10.00	86.58

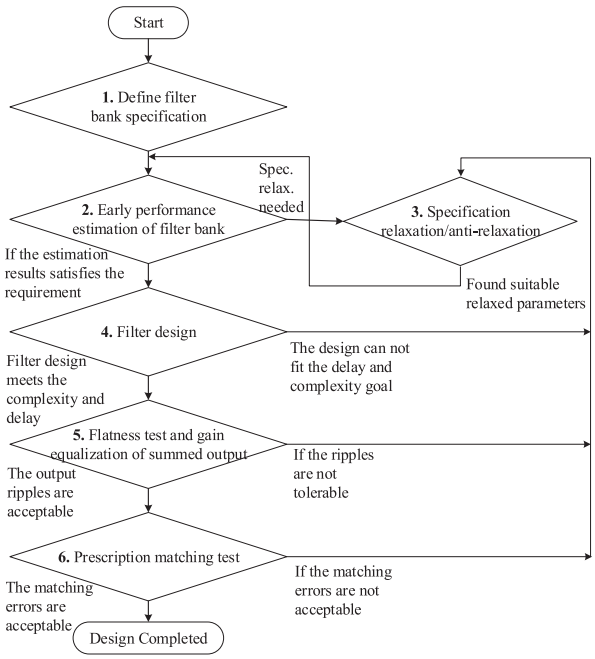

Fig. 6. Design flow procedure.

for hearing aid applications, the maximum delay constraint, the allowable ripple of summed output signals, and the acceptable prescription matching error should be determined.

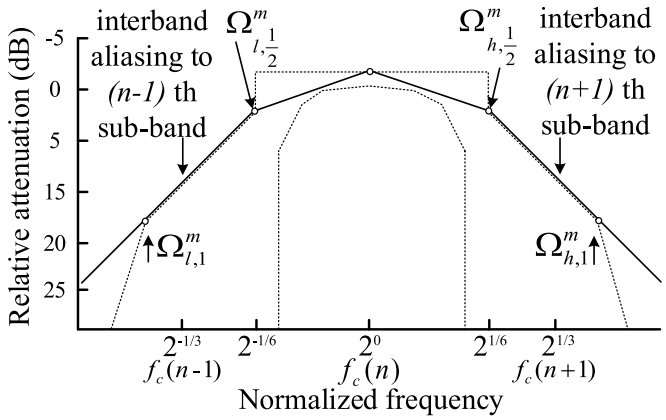

Fig. 7. Piecewise linear slope for filter prediction. The solid lines represent predicted filter, and the dotted lines are relative attenuation.

2) Early Performance Estimation of Filter Bank: The purpose of this stage is to predict the performance of the filter bank according to the given (relaxed) specification and constraints to avoid unnecessary trials and unachievable constraints. The most significant performance index for estimating the filter bank is the inter-band aliasing interference, which will affect the delay/complexity of the filters, the ripples of summed output signals, and the prescription matching capability. We predict the response of the filter bank using piecewise lines in the frequency domain, starting from the passband to the stopband. The solid lines in Fig. 7 represent the predicted filter response. The predicted filter response can be divided into two sections, and each of them has its own slope. The first section starts from the mid-band point ($f_c(n)$, min. attenuation $= -0.5$ dB) to the band edge points ($\Omega^m_{h,\frac{1}{2}}$, $\Omega^m_{l,\frac{1}{2}}$, min. attenuation $= +1.6$ dB). Additionally, the second section is from the band edge points to the break points of ($\Omega^m_{h,1}$, $\Omega^m_{l,1}$, max. attenuation $\approx +13.5$ dB). After the distance between the mid-band frequency and the observing point(s) has been obtained, the predicted interband aliasing at the observing point can be

determined using the product of the predicted slope and the distance in the frequency axis. An example is presented here to demonstrate the interband aliasing prediction. Consider a standard ANSI S1.11 1/3-octave specification; one needs to predict F_{22}'s interband aliasing contributed to F_{23}. For simplicity, the frequency scale is normalized to $f_c(22)$ (at -0.5 dB), the F_{22}'s band edge frequency $f_h(22)$ is 1.12 (at 1.6 dB), and F_{23}'s mid-band frequency becomes 1.26. The slopes of the first and second sections are 17.5 and 87.6 dB/nf (decibel per normalized frequency), respectively. F_{23}'s mid-band frequency clearly lays off the passband of F_{22} $(1.26 > 1.12)$, as shown in the right-hand side of Fig. 7. Therefore, the interband aliasing on F_{23} can be linearly interpolated from the second section of $\Omega_{h,\frac{1}{2}}$ $(1.12, +1.6\ \text{dB})$ and $\Omega_{h,1}$ $(1.29, +16.5\ \text{dB})$. Then, the predicted interband aliasing of F_{22} contributed to F_{23} is $1.6 + (1.26 - 1.12) \times 87.6 = +13.8$ dB.

Note that if the hearing aid is designed for a specific patient, then the maximum gain difference and the maximum interband gain differences of the filter bank should be extracted from the corresponding prescription. The maximum gain difference indicates the required minimum stopband attenuation for the subfilters. For the class-2 specification [9], the allowable maximum gain difference is 60 dB. Moreover, the maximum interband gain differences are calculated from the largest interband gain differences according to specific or typical hearing-loss patients' prescribed gains. They imply the maximum interband aliasing permissible for the desired filter bank specification. The suggested predicted interband aliasing could have a tolerable error of $+0.5 \sim +3$ dB compared to the maximum interband gain differences. However, it is only valid when both adjacent subbands cover in their passband region, and the interband gain differences should be less than 6 dB. (The filter response of the class-2 specification will be limited to the range of +0.5 dB to -5.5 dB.) If required maximum interband gain differences are greater than 6 dB in this case, it is difficult for the filter bank to accomplish the prescription matching requirement, i.e., ± 1.5 dB errors. Subsequently, anti-relaxation of the filter specification or an increase of the filter's tap length is needed. After extracting these two features, we are able to select suitable relaxed parameters and estimate the interband aliasing by piecewise linear slope prediction. If the predicted interband aliasing is suitable, then it continues to step 4 for designing the filter bank. Otherwise, the procedure moves to step 3 to re-select the relaxed parameters. In addition, if the maximum gain difference is greater than 60 dB or then maximum interband gain differences are larger than 13.5 dB, then stricter specifications should be used, i.e., class-1 or class-0 rather than class-2.

3) Specification Relaxation/Anti-Relaxation: The specification relaxation of the ANSI S1.11 filter bank has two objectives. The first is to meet the delay constraint, and the other is to decrease the complexity with allowable interband aliasing interference. Because filter F_{22} has the narrowest transition bandwidth, to retain the octave property and delay constraint, we select appropriate α-series parameters (α_h^m, α_l^m) for passband expansion such that a proper filter design for the relaxed F_{22} can be found. The ratio of the α-series parameters can be arbitrarily chosen depending on the desired requirement. After the expansion parameters are determined, the (expansion) parameters for the next sub-filter can be calculated by

$$\alpha_h^m(n) = \alpha_h^m(n-1) \times 2^{-1/b} \tag{11}$$

and

$$\alpha_l^m(n) = \alpha_l^m(n-1) \times 2^{-1/b}. \tag{12}$$

The α-series parameters contract $2^{1/b}$ times compared to the previous ones to prevent the expanded bandwidth from increasing with mid-band frequency. This result can be verified by substituting the parameters into (4).

To reduce the complexity by shortening the filter length with acceptable matching error, we keep the ANSI S1.11 specification in the passband valid but release the limitations on the stopband-to-passband transition. This type of specification relaxation is controlled by β-series parameters, i.e., (β_h^m, β_l^m). The larger the values, the more overlap of each sub-band. Consequently, the β-series parameters are selected depending on the allowable interband aliasing interference. The β-series parameters can then be applied with the same values to each sub-band as those in (11) and (12), i.e.,

$$\beta_h^m(n) = \beta_h^m(n-1) \times 2^{-1/b} \tag{13}$$

and

$$\beta_l^m(n) = \beta_l^m(n-1) \times 2^{-1/b}. \tag{14}$$

After determining the relaxed specification, we will return to step 2 to estimate the performance of the filter bank.

4) Filter Design: The heuristic filter coefficient design flow provided in [14] is a recommended and suitable approach because the objective of the filter design algorithm in [14] is to search the optimized coefficients for the given ANSI S1.11 specification and constraints, which include filter complexity, passband ripples, stopband attenuation, and anti-aliasing issue for multi-rate processing. In this paper, however, the following case designs did not directly adopt this algorithm but were rather primarily based on previous works' [14], [15] parameters and configurations. If another filter design flow is used, the major concern is to maintain the linear-phase property of the resulting filters. After the specification from step 2 is determined, all the sub-filters should meet the requirement of the desired relative attenuation according to the relaxed parameters. Then, the delay d_n and the complexity (or cost) c_n of sub-filter F_n can be examined by

$$d_n = \sum_i^K \left(\frac{N_i - 1}{2}\right)\left(\frac{f_s}{f_{s_i}}\right) = d_{f_n} + d_{r_n} \le d_s \tag{15}$$

and

$$c_n = \sum_i^K \left(\frac{N_i + 1}{2}\right)\left(\frac{f_{s_i}}{f_s}\right) = c_{f_n} + c_{r_n}, \tag{16}$$

assuming that, for multi-stage, multi-rate filter implementation, there are K filters with tap length N_i, sampling rate f_{s_i}, $1 \le i \le K$, and N_i's are odd. Please note that both d_n and c_n can be divided into two parts: one is contributed by the passband filter, denoted by d_{f_n} and c_{f_n}, respectively, and the other

is from the rate conversion, i.e., d_{r_n} and c_{r_n}. Indeed, the rate conversion part contributes no effect on the sub-band filtering, but it helps in altering the sampling rate and provides a suitable ratio for designing a recursive FIR filter bank architecture. Sharing rate conversions, similar to that in [18], can reduce the complexity induced by SRCs, and a larger rate conversion does improve the benefit of reducing complexity and the sub-band's operating rate. However, the penalty is the induced latency. Referring to Section III, we have developed an efficient multi-rate architecture for an ANSI-like FIR filter bank. If the sub-filter cannot satisfy the given specification or violates the delay constraint after exhaustive trials, the next step is to go to step 3 for specification relaxation; otherwise, it proceeds to step 5.

5) Flatness Test and Gain Equalization of Summation Output Signals: The flatness test checks the ripples on the summation of the output sub-band signals. This examination reflects the loudness distortion generated by the system-relaxed filter bank. The class-2 specification has defined that the ripples of summed output signals should be within ± 0.5 dB [9]. However, the ripples increase when the filters overlap more with each other, such as the quasi-ANSI filter [15]. To minimize the ripples, we apply the equalized gain, denoted by $g(n)$, to the nth sub-filter to improve the performance of the filter bank. We generalize the formula for calculating the ripples of summed output signals from the ANSI S1.11 specification as shown in

$$\Delta P(n) = 10log(10^{0.1\times g(n)} + \sum_i 10^{-0.1\times A(n,i)}), \qquad (17)$$

where $A(n,i)$ is the magnitude measured at mid-band frequency $f_c(n)$. Note that $\Delta P(n)$ checks the levels (in dB) around each mid-band frequency of the filter bank. For simplicity, we ignore the ones whose magnitude at the specified mid-band frequency contributes less than -10 dB. Then, all the $\Delta P(n)$ should be less than the maximum tolerance ripple. One can obtain a suitable $g(n)$ from (17) to minimize the ripples by using constrained non-linear multi-variable optimization tools, e.g., *fmincon* in MATLAB [24]. Meanwhile, the maximum and minimum of equalized gains $g(n)$ should be constrained to prevent the sub-band signals from being less significant or overridden by the noise.

Fig. 8 is an example of the proposed gain equalization process. As shown in Fig. 8(a), the interband aliasing contributions to F_{24} are generated by F_{22}, F_{23}, F_{25}, and F_{26}, respectively, which are represented by $A(24,-2)$, $A(24,-1)$, $A(24,+1)$, and $A(24,+2)$. Because its aliasing component is less than -10 dB, the interferences from sub-filers F_{22} and F_{26} are less significant to the ripple on F_{24} and can be ignored. By (17), the equalized gain $g(24)$ for minimum ripple at F_{24} is 2.94 dB, which makes $\Delta P(24) = 0$. Note that the ripple at F_{24} is correlated with $g(23)$, $g(24)$, and $g(25)$ because of increased passband or overlapped transition bandwidth. Therefore, we use (17) as the objective function and adopt the tool *fmincon* in MATLAB [24] to flatten the summed output response as the solid curve shown in Fig. 8(b). The suggested ripples after applying equalized gains need to be smaller than $\pm 0.5 \sim 1.5$ dB [9].

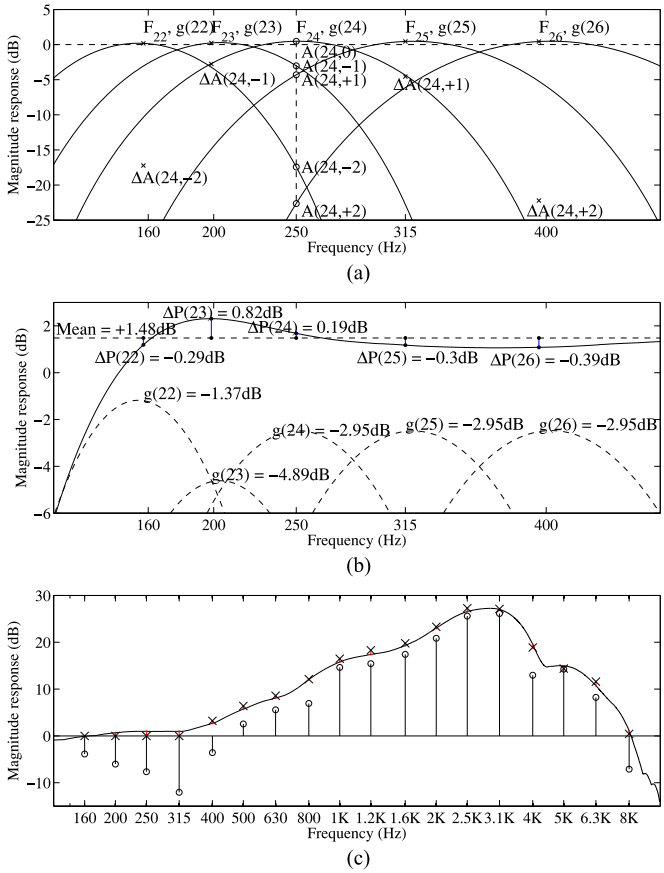

Fig. 8. Demonstration of gain equalization and prescription matching for the proposed filter bank: (a) estimation and ripple minimization for sub-band F_{24} and (b) summed magnitude response after gain equalization. (c) Patient 1's prescription matching result using the proposed filter bank

6) Prescription Matching Test: In this study, the well-known prescription matching formula NAL-NL1 [10] is considered. Using the NAL-NL1 formula, the audiogram measured from a patient with mild hearing loss [see Fig. 9(a)], as well as a patient with moderately severe hearing loss [see Fig. 9(b)], can be converted into several compensated prescriptions at different sound pressure levels in accordance with the intelligibility and loudness models. Similarly, we derive objective functions for using constrained multi-variables optimization tools [24] to find the optimized prescribed gains for hearing aids. The analytic prescription matching error $E(n)$ of the nth sub-filter is

$$E(n) = 10log\left(\frac{1 + 10^{0.1\times I(n)} + \sum_{i\neq n} 10^{0.1\times(I(i)-\Delta A(n,i))}}{1 + 10^{0.1\times I_g(n)}}\right), \qquad (18)$$

where $I(n)$ is the final prescribed gain, $I_g(n)$ is the targeted prescribed gain from NAL-NL1 formula [10], and $\Delta A(n,i)$ is the magnitude difference between the nth and $(n+i)$th mid-band frequencies (in dB). The targeted prescribed gains $I_g(n)$ from NAL-NL1 cannot apply directly on the relaxed ANSI S1.11 filter banks because of the increased inter-band interference. The second term in the numerator of (18) yields the magnitude increases on the nth sub-band by $I(n)$, and the third term is the

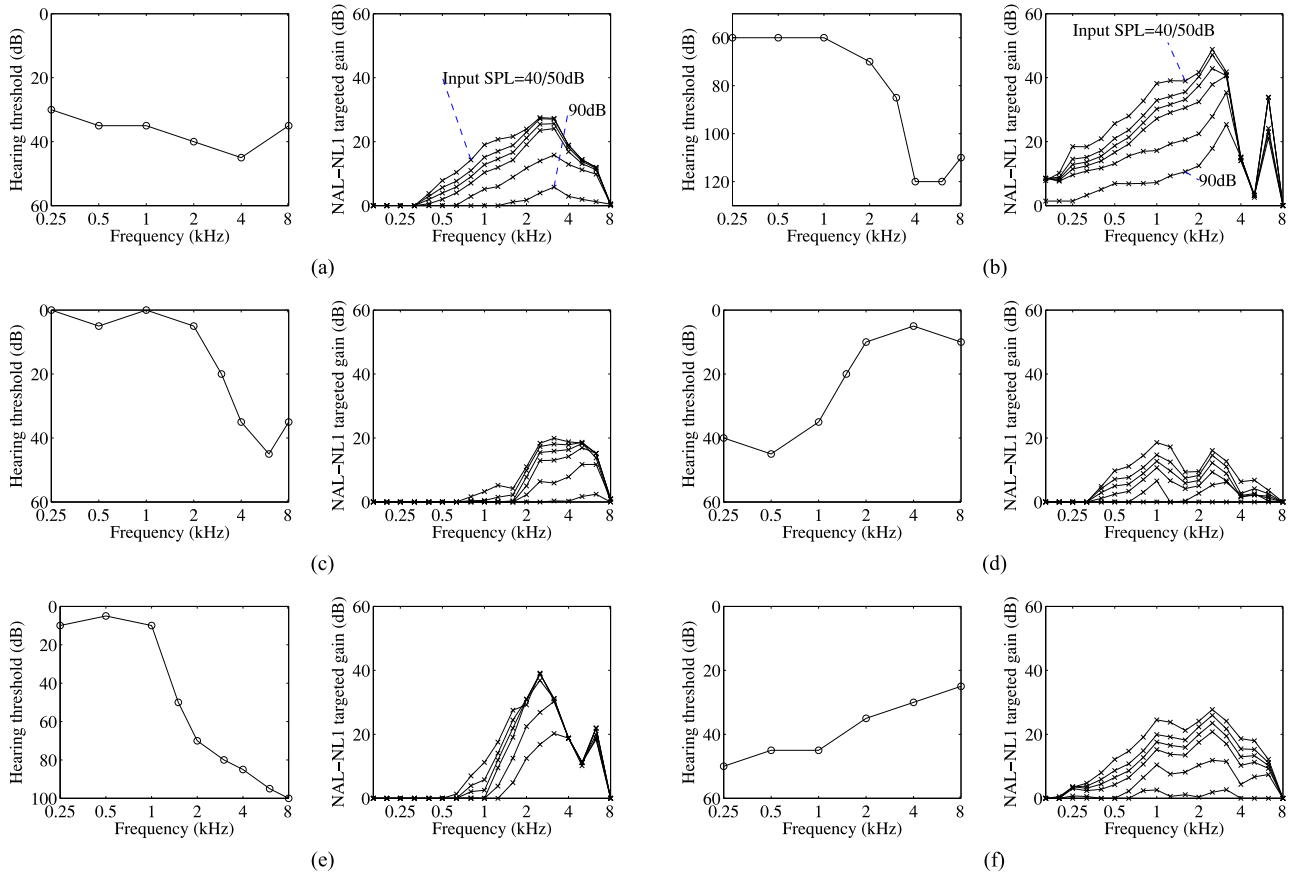

Fig. 9. Hearing threshold and NAL-NL1 targeted gain of patients 1 to 6. (a) Patient 1, flat with mild hearing loss. (b) Patient 2, steeply sloping high-frequency loss with moderate-severe hearing loss. (c) Patient 3, mild hearing loss in high frequency. (d) Patient 4, moderate hearing loss in low frequency. (e) Patient 5, steeply sloping with moderately-severe hearing loss. (f) Patient 6, reverse sloping with moderate hearing loss.

aliasing component contributed at the nth mid-band frequency. For simplicity, we can rewrite (18) into

$$\hat{E}(n) = \left(\frac{1 + \hat{I}(n) + \sum_{i \neq n} \Delta\hat{A}(n,i) \times \hat{I}(i)}{1 + \hat{I}_g(n)} \right), \qquad (19)$$

where $I(n)$, $I_g(n)$, and $\Delta A(n,i)$ are transformed to magnitude scale and the right-hand side of (18) is converted to $10^{0.1 \times E(n)}$ instead. Theoretically, we might expect the matching errors $\hat{E}(n)$ to become zero. The prescribed gains $\hat{I}(n)$ should be determined by $\hat{I}_g(n)$ and the aliasing component $\Delta\hat{A}(n,i)$ as

$$\hat{I}(n) + \sum_{i \neq n} \Delta\hat{A}(n,i) \times \hat{I}(i) = \hat{I}_g(n). \qquad (20)$$

In practical cases, we cannot obtain the exact solution from (20) directly. Rather, we use a multi-variable optimization tool, i.e., *fmincon* in MATLAB [24], to find the non-trivial solutions that minimize the matching errors in (18).

After many iterations from step 2 to step 6, a desired design that satisfies the requirements of the delay, complexity, prescription matching capability, and system-wide consideration is obtained. Before leaving this section, we note that Fig. 8(c) is one of prescription matching results, where the crosses represent the NAL-NL1 targeted gains, the circles represent the final prescribed gains applied on each sub-band, and the solid curve is the prescribed summed output response within 1 dB error with respect to the targeted gains.

IV. Design Example and Result

In this section, several design examples, namely, the delay-oriented cases, complexity-oriented cases, and patient-oriented cases, are presented to demonstrate the success of the proposed design procedure. At the end of this section, four additional typical audiograms are presented to show the matching capability of each design. The additional audiograms include mild loss in high frequency (patient 3), moderate loss in low frequency (patient 4), moderately severe with precipitous sloping (patient 5), and moderate loss with reverse sloping (patient 6). The audiograms and corresponding target gains are shown in Fig. 9. If readers need to select another set of audiograms, Giletti's and Flamme [25] and Lai's [26] works are appropriate references for readers to choose representative audiometric configurations.

A. Delay-Oriented Cases

We apply the design considerations of less than 10 ms delay constraint, ± 1.0 dB ripples, and ± 1.5 dB matching errors to compare with the quasi-ANSI filter bank [15]. From (11)–(14), we first obtain the appropriate set of relaxed parameters (α_l^m, α_h^m, β_l^m, β_h^m), as listed in the second major column of Table III,

TABLE III
DETAILED INFORMATION OF PROPOSED A1 DESIGN

nth	α_l^m	α_h^m	β_l^m	β_h^m	Cascaded Multirate Filters			MPY per sample			Delay (ms)
F_{22}	0.2200	0.010	0.2500	0.2500	[IA_2,↓4]	[H_{22}]	[↑4,IS_2]	6.25	12.25	6.25	10.00
F_{23}	0.1760	-	0.2000	0.2000	[IA_2,↓4]	[H_{23}]	[↑4,IS_2]	6.25	12.25	6.25	10.00
F_{24}	0.1408	-	0.1600	0.1600	[IA_2,↓4]	[H_{24}]	[↑4,IS_2]	6.25	10.50	6.25	8.83
F_{25}	0.1126	-	0.1200	0.1200	[IA_2,↓4]	[H_{25}]	[↑4,IS_2]	6.25	10.00	6.25	8.50
F_{26}	0.0090	-	0.1024	0.1024	[IA_2,↓4]	[H_{26}]	[↑4,IS_2]	6.25	9.75	6.25	8.33
F_{27}	0.0072	-	0.0819	0.0819	[IA_2,↓4]	[H_{27}]	[↑4,IS_2]	6.25	8.50	6.25	7.50
F_{28}	0.0057	-	0.0655	0.0655	[IA_2,↓4]	[H_{28}]	[↑4,IS_2]	6.25	7.75	6.25	7.00
F_{29}	0.0046	-	0.0524	0.0524	[IA_2,↓4]	[H_{29}]	[↑4,IS_2]	6.25	6.25	6.25	6.00
F_{30}	0.0036	-	0.0419	0.0419	[IA_2,↓4]	[H_{30}]	[↑4,IS_2]	6.25	5.00	6.25	5.17
F_{31}	-	-	-	-	[HA_2,↓(8/5)] [$IA"_2$,↓4]	[H_{39}]	[↑4,$IS"_2$] [↑(8/5),HA_2]	7.25	2.50	2.19 2.50 5.75	8.80
F_{32}	-	-	-	-	[HA_1,↓(5/4)] [IA'_2,↓4]	[H_{39}]	[↑4,$IS"_2$] [↑(5/4),HA_1]	7.50	4.20	2.80 4.20 6.20	6.88
F_{33}	-	-	-	-	[IA_2,↓4]	[H_{39}]	[↑4,IS_2]	6.25		3.50 6.25	4.17
F_{34}	-	-	-	-	[HA_2,↓(8/5)] [$IA"_1$,↓2]	[H_{39}]	[↑2,$IS"_1$] [↑(8/5),HA_2]	7.25	3.13	4.38 3.13 5.75	6.27
F_{35}	-	-	-	-	[HA_1,↓(5/4)] [IA'_1,↓2]	[H_{39}]	[↑2,IS'_1] [↑(5/4),HA_1]	7.50	5.20	5.60 5.20 6.20	5.31
F_{36}	-	-	-	-	[IA_1,↓2]	[H_{39}]	[↑2,IS_1]	7.50		7.00 7.50	2.25
F_{37}	-	-	-	-	[HA_2,↓(8/5)]	[H_{39}]	[↑(8/5),HA_2]	7.25		8.75 5.75	4.20
F_{38}	-	-	-	-	[HA_1,↓(5/4)]	[H_{38}]	[↑(5/4),HA_1]	7.50		11.20 6.20	2.76
F_{39}	-	-	-	-		[H_{39}]				14.00	0.54

Rate conversion filters	Conversion rate	Operating frequency f_s (Norm. to Fs)	Anti-aliasing filter tap length	Delay (ms)	MPY per sample (Polyphase [19])
HA_1	(4/5) , (5/4)	1	51	1.04	7.50 , 6.20
HA_2	(5/8) , (8/5)	1	81	1.67	7.25 , 5.75
IA_1, IS_1	(1/2) , 2	1	29	0.58	7.500
IA_1', IS_1'	(1/2) , 2	4/5	25	0.63	5.200
IA_1", IS_1"	(1/2) , 2	5/8	19	0.60	3.130
IA_2, IS_2	(1/4) , 4	1	49	1.00	6.250
IA_2', IS_2'	(1/4) , 4	4/5	41	1.04	4.200
IA_2", IS_2"	(1/4) , 4	5/8	31	1.00	2.500

TABLE IV
PATIENT 1'S PRESCRIPTION ANALYSIS AND PREDICTED/MEASURED INTERBAND ALIASING BY RELAXED PARAMETERS

nth sub-bands	Max. interband gain differences (dB)	Relaxed parameters α_l^m	α_h^m	β_l^m	β_h^m	Pred./Meas. ave. interband aliasing (dB)
22	0	0.400	0.400	1.000	0.800	–/−0.14
23	0	0.320	0.320	0.800	0.640	−0.62/−1.00
24	0	0.256	0.256	0.640	0.512	−0.82/−1.18
25	3.78	0.204	0.204	0.512	0.409	−1.04/−1.09
26	4.60	0.163	0.163	0.409	0.327	−1.27/−1.69
27	2.53	0.131	0.131	0.327	0.262	−1.51/−2.70
28	3.88	0.104	0.104	0.262	0.209	−2.22/−3.83
29	4.73	0.083	0.083	0.209	0.167	−3.27/−4.17
30	1.86	0.067	0.067	0.167	0.134	−4.34/−5.56
31 ∼ 39	1.81 ∼ 11.99	–	–	–	–	−11.20/−16.42

TABLE V
EARLY PREDICTED AND MEASURED INTERBAND ALIASING FOR THE $A1$ DESIGN

	Predicted(dB)			Measured(dB)		
nth sub-filter	(n − 1)	(n + 1)	Average	(n − 1)	(n + 1)	Average
22	–	−0.8	–	–	−3.2	–
23	−1.0	−1.4	−1.20	−3.0	−3.0	−3.00
24	−1.2	−1.3	−1.25	−2.7	−4.3	−3.50
25	−1.4	−1.5	−1.45	−4.3	−5.2	−4.75
26	−2.3	−3.5	−2.90	−6.1	−7.2	−6.65
27	−4.4	−5.5	−4.95	−7.2	−7.8	−7.50
28	−6.2	−7.1	−6.65	−8.7	−8.0	−8.35
29	−7.7	−8.3	−8.00	−9.3	−9.2	−9.25
30	−8.9	−9.3	−9.10	−10.2	−10.9	−10.55
31-39	−13.7	−13.4	−15.40	−15.3	−16.0	−15.65

and the targeted interband aliasing is set to 3 dB. Based on the piecewise linear slope prediction approach, the interband aliasing interference can be estimated (see Table V). For the nth sub-filter, there are two predicted interband aliasing interferences listed in Table V, which contributes to its previous, i.e., the $(n-1)$th, sub-filter and the next $(n+1)$th sub-filter. For simplicity, we used the average of two estimated values as the predicted interband aliasing interference. The predicted average interband aliasing interference at F_{23} is -1.2 dB on average (see Table V), which is within the tolerable error of 3 dB and sufficient to fit most of the targeted prescriptions in the low-frequency range because the prescribed gains in the low-frequency range do not change dramatically in most types of hearing-loss (see Fig. 9).

To apply the proposed hybrid multirate architecture in Fig. 5 to realize the system-relaxed quasi-ANSI FIR filter bank, anti-aliasing filters HA_i, IA_i, IA_i', and IA_i'', $i = 1, 2$, are required. From the experimental results in [15], the decimate-by-4 or interpolate-by-4 SRC accompanies the $\pi/4$ cut-off frequency anti-aliasing filter, i.e., the IA_2 in Fig. 5, whose filter length is 49 and contributes a 1 ms delay. Therefore, the delay budget of filter H_1 in Fig. 5 is left by 8 ms. Consequently, the maximum length of H_1 is 97, which is the same as that in [15]. With the efficient polyphase implementation [19], the computational complexity (in terms of MPY/S) of IA_2 is $\frac{1}{2} \times \left(\frac{49+1}{4}\right) = 6.25$. Similarly, the MPY/S of H_1 is 12.25 (see Table III). The detailed information of each sub-filter and the required anti-aliasing filters are listed in Table III. For convenience, this FIR filter bank is referred to as the $A1$ design hereafter. The tap lengths of sub-filters $H_1 \sim H_9$ and H_{18} of the $A1$ de-

TABLE VI
TAP LENGTH OF SUB-FILTERS IN EACH CASE

	A1	A2	A3	B1	B2	P1	P2
H_{22}	97	97	63	97	85	49	217
H_{23}	97	97	63	93	73	43	183
H_{24}	83	83	53	81	61	37	147
H_{25}	79	79	51	67	59	43	119
H_{26}	77	77	51	63	51	37	99
H_{27}	67	67	43	53	41	37	81
H_{28}	61	61	39	47	37	33	81
H_{29}	49	49	31	39	31	29	65
H_{30}	39	39	27	31	27	25	53
H_{37}	–	45	–	–	–	–	–
H_{38}	–	33	–	–	–	–	–
H_{39}	27	27	27	21	15	21	27

TABLE VII
PATIENT 2'S PRESCRIPTION ANALYSIS AND PREDICTED/MEASURED INTERBAND ALIASING BY RELAXED PARAMETERS

		Relaxed parameters				
nth sub-bands	Max. interband gain differences (dB)	α_l^m	α_h^m	β_l^m	β_h^m	Pred./Meas. ave. interband aliasing (dB)
22	9.80	0.060	0.030	–	–	−/−10.39
23	9.43	0.048	0.024	–	–	−9.78/−11.40
24	1.51	0.038	0.019	–	–	−10.57/−11.98
25	1.48	0.030	0.015	–	–	−11.19/−12.70
26	4.64	0.024	0.012	–	–	−11.69/−13.06
27	2.97	0.019	0.009	–	–	−12.08/−14.25
28 ∼ 39	1.58 ∼ 15.58	–	–	–	–	−13.59/−15.76

sign in Fig. 5 are listed in Table VI. The delay of the sub-filter can be calculated by (15). For example, for F_{22}, the delay is $\left(\frac{49-1}{2}\right)\left(\frac{1}{2}\right)+\left(\frac{97-1}{2}\right)(4)+\left(\frac{49-1}{2}\right)\left(\frac{1}{2}\right)=240$, which is equal to 10 ms for the 24 kHz sampling frequency. Similarly, the delay of the other sub-filter of the $A1$ design can be calculated and is listed in the last column of Table III. Moreover, the measured interband aliasing interference of each sub-filter is presented in the last major column of Table III for comparison.

As shown in Table III, the MPY/S of the $A1$ design is only 226, which saves approximately 11.4% of the complexity of the quasi-ANSI filter bank with the same hybrid multirate architecture (see Table II). As expected, the proposed system-relaxed Nyquist ANSI filter bank outperforms the previous one [15] while achieving the same design considerations. For later discussions, we implement another two designs of the proposed systematic relaxed Nyquist ANSI filter bank with different architectures: the single-stage multirate architecture in [15], namely, the $A2$ design, and the multiple-stage multirate architecture in [18], i.e., the $A3$ design. The tap lengths of the required sub-filters of the $A2$ design and of the $A3$ design are also listed in Table VI for comparison. The MPY/S of the $A3$ design is 177; however, the delay is up to 13.6 ms.

B. Complexity-Oriented Cases

Continuing with the $A1$ design, one might desire to decrease the complexity as low as the $A2$ or $A3$ design but while maintaining the sampling rate reduction, i.e., 86.58%, and the 10 ms delay constraint. The solution of no extra delay introduced by the additional rate conversion process is to relax the passband-to-stopband regulation of sub-filters, which is controlled by the β-series parameters. The increase of the passband-to-stopband transition causes the filter's tap length to shorten. Therefore, the complexity reduction goals from $A1$ to $A2$ or $A3$ design can be achieved by reducing all sub-filters' tap lengths by approximately 15% or 30% on average. After a few trials from steps 1 to 4, the relaxed parameter in the proposed $A1$ design should be globally added by $(\Delta\beta_l^m, \Delta\beta_h^m) = (0.1, 0.0)$ and $(0.3, 0.1)$. The globally added relaxed filter banks are named the $B1$ design and $B2$ design, respectively. Applying the same design procedures, the estimated interband aliasing interference degrades less than 1 dB for the $B1$ design and 2 dB for the $B2$ design. The tap lengths of the required sub-filters of the $B1$ and $B2$ designs are listed in Table VI. The MPY/S of the $B1$ design is 204, whereas that of the $B2$ design is 178.

C. Patient-Oriented Cases

If the hardware of the hearing aid is programmable, one could design a customized, low-delay, and high-performance, system-relaxed ANSI Nyquist filter bank for an individual patient. Two typical patients' prescriptions are considered: a mild hearing-loss patient with a flat audiogram (patient 1, *P1*) and a moderately severe hearing-loss patient with a sloping audiogram (patient 2, *P2*). The audiograms of $P1$ and $P2$ and their corresponding NAL-NL1 prescribed insertion gains are shown in Fig. 9. In addition, referring to the tolerable delay experiment for hearing-impaired patients, the result in [27] revealed that the patient with more severe hearing loss has a longer tolerable delay. Hence, we determined that the delay constraints for $P1$ and $P2$ are 10 and 20 ms, respectively. Given the NAL-NL1 prescriptions of $P1$ and $P2$, the allowable maximum interband gain difference of each sub-filter can be derived, which are described in the second columns of Table IV and VII, respectively. Recalling the predicted interband aliasing interference in step 3 for early estimation, if the interband aliasing of each sub-filter is greater than its maximum interband gain difference, then the filter bank would guarantee a smaller matching error. After a few iterations from step 2 to step 6, we select the adequate relaxed parameter sets: $(\alpha_l^m, \alpha_h^m, \beta_l^m, \beta_h^m) = (0.4, 0.4, 1.0, 0.8)$ for patient $P1$ and $(0.06, 0.03, 0.0, 0.0)$ for $P2$. With the system-relaxed parameters, the predicted/measured average interband aliasing interferences are summarized in Table IV for $P1$ and in Table VII for $P2$. The tap lengths of the required sub-filters of the $P1$ and $P2$ designs, respectively, are also listed in Table VI. The MPY/S of the $P1$ design is 174, whereas that of the $P2$ design is 276.

D. Comparison Results

We use both the design results in Table VIII and the prescription matching capability in Table IX to perform fairly comprehensive comparisons between the proposed Ai, Bi, and Pi designs and previous works, i.e., $S1$ [14], $Q1$ [15], and $Q2$ [18],

TABLE VIII
DESIGN COMPARISONS

Design	MPY	# of filters required	Total coef.	Latency (ms)	Sub-band sampling rat. reduct.	Ripples (dB)
S1 [14]	140	5	88	78.37	78%	0.33
Q1 [15]	226	14	506	10.00	100%	0.90
Q2 [18]	192	20	451	13.58	75%	0.90
A1	226	20	579	10.00	86%	0.82
A2	202	14	412	10.00	100%	0.82
A3	177	20	465	13.60	75%	0.82
B1	204	20	536	10.00	86%	0.79
B2	178	20	480	9.00	86%	0.76
P1	174	20	418	6.00	86%	1.05
P2	276	20	777	20.00	86%	0.59

TABLE IX
PRESCRIPTION MATCHING TEST RESULTS

Design (mean $\pm$ std.)	S1	Qi	Ai	B1	B2	P1	P2
Patient 1	0.00	-0.08	-0.05	-0.17	-0.53	-0.27	0.00
	± 0.00	± 0.26	± 0.16	± 0.40	± 0.87	± 0.57	± 0.00
Patient 2	0.00	-0.20	-0.20	-0.19	-0.53	-0.39	-0.00
	± 0.00	± 0.89	± 0.76	± 0.85	± 0.87	± 1.14	± 0.06
Patient 3	0.00	-0.05	-0.04	-0.17	-0.67	-0.04	0.00
	± 0.05	± 0.17	± 0.13	± 0.40	± 0.95	± 0.32	± 0.02
Patient 4	0.00	-0.07	-0.04	-0.16	-0.50	-0.23	0.00
	± 0.00	± 0.21	± 0.14	± 0.38	± 0.95	± 0.61	± 0.00
Patient 5	0.00	-0.05	-0.08	-0.19	-0.80	-0.18	0.00
	± 0.06	± 0.16	± 0.29	± 0.42	± 1.24	± 0.65	± 0.07
Patient 6	0.00	-0.13	-0.07	-0.13	-0.18	-0.15	0.00
	± 0.00	± 0.50	± 0.28	± 0.47	± 0.53	± 0.47	± 0.00
Overall average	0.00	-0.10	-0.08	-0.17	-0.53	-0.21	0.00
	± 0.01	± 0.37	± 0.29	± 0.49	± 1.02	± 0.63	± 0.02

in terms of delay, complexity, performance, and system-wide effectiveness to conclude this section.

The three filter banks, namely, $A1$, $A2$, and $A3$, are designed with the same system-relaxed ANSI specification but with different multirate architectures. The Ai designs have slightly better ripples and matching errors than the quasi-ANSI filters $Q1$ [15]. However, the proposed $A2$ design saves approximately 11% of the computational complexity of that in $Q1$. Among the three proposed Ai designs, the complexity and the performance of the sampling rate reduction of the $A3$ design are superior, but the latency is 13.6 ms, whereas the $A1$ and $A2$ designs are compromised by the complexity and sampling rate reduction with a strictly constrained delay of 10 ms. With the worst sampling rate reduction, the $A2$ design is suitable for a simple hearing aid system with non-aggressive speech enhancement algorithms, such as [28]. In the future, the multi-channel WDRC and more active speech enhancement algorithms will be imperative. With sampling rate reduction, the $A1$ or $A3$ design will be the appropriately efficient system-relaxed Nyquist ANSI filter bank for hearing-aid systems.

To decrease the complexity as low as possible while maintaining the same performance of the sampling rate reduction and latency, the design of $B1$ or $B2$, respectively, suffers more matching errors on average, i.e., -0.17 ± 0.49 dB or -0.53 ± 1.02 dB, respectively, to the prescription of patient $P1$ because of the expanded passband bandwidth. With the system-relaxed specifications, note that the ripples of the summed output signal of the proposed Ai designs outperform that of $Q1$. The proposed system-relaxed parameters control the sub-filters to be expanded regularly, which helps better prescription matching capability. This is why the prescription matching error of the $A1$ design is superior to $Q1$.

The complexity of the $B2$ and $P1$ designs are comparable but quite different from their matching errors, i.e., -0.53 ± 1.02 versus -0.21 ± 0.63 dB. The reason is that the $B2$ design applies a complexity-oriented approach with a stretched transition bandwidth, whereas the $P1$ design uses the linear slope estimation to carefully select appropriate system-relaxed parameters. Therefore, the prescription matching capability of the $P1$ design is superior. A similar result arises when comparing the $A2$ design with the $B1$ design.

Finally, $P2$ is designed for patient 2, who is moderately severe with sloping hearing-loss, and it has equal matching capability within 0.1 dB compared to $S1$ in this patient. Obviously, $P2$ is more feasible than $S1$ for real-time processing hearing aids. However, the latency is still too long to address acoustic feedback problems for general scenarios. The use of such filter banks will be restricted. The recommended latency should be reduced within 10 ms. Then, the second candidate would be the Ai design with an acceptable matching error of -0.20 ± 0.89 dB.

V. CONCLUSION

In this paper, we have presented a systematic relaxed ANSI S1.11 specification and proposed a design procedure concerning delay, complexity, performance, and system-wide effectiveness, resulting in an optimized multirate filter bank according to the requirements of hearing aid systems. The contributions of this paper are as follows: 1) Systematic relaxation with controllable parameters on the ANSI S1.11 specification. 2) Early prediction or performance evaluation with the piecewise linear slope approach avoids unnecessary trials and approaches for the optimized design. 3) Extracting the key performance indices of sub-filters to systematically optimize the ripples of summed output and prescription matching errors. 4) System-wide consideration for selecting an adequate system-relaxed Nyquist ANSI filter bank. Moreover, seven design cases with different system requirements are presented to demonstrate the success of the proposed design procedure. Considering highly integrated hearing aid systems with sophisticated DSP algorithms, the design of the filter bank is not considered in terms of only the latency and the computational complexity. The performance of the sampling rate reduction should clearly be included. We believe that the proposed system-relaxed Nyquist ANSI filter bank provides a foundation for future academic and clinical research and not limited to hearing aids. Based on the proposed design procedure, the optimized multirate architecture can easily be implemented in either software or hardware. It does break the barrier between filter bank specifications and practical hardware implementation. In addition, it provides us with the idea that future hearing aids would be able to select an optimized filter bank from a built-in database in response to various acoustic scenarios.

REFERENCES

[1] J. M. Kates, *Digital Hearing Aids*. San Diego, CA, USA: Plural Publishing, 2008.

[2] S. C. Lai, C. H. Liu, L. Y. Wang, S. H. Chen, and K. H. Chen, "11.25-ms-group-delay and low-complexity algorithm design of 18-band quasi-ansi s1.11 1/3 octave digital filterbank for hearing aids," *IEEE Trans Circuits Syst. I*, vol. 62, no. 6, pp. 1572–1581, Jun. 2015.

[3] J. M. Kates, "Dynamic-range compression using digital frequency warping," in *Proc. 37th Asilomar Conf. Signals, Syst. Comput.*, Nov. 2003, vol. 1, pp. 715–719.

[4] M. Parfieniuk and A. Petrovsky, "Warped dft as the basis for psychoacoustic model," in *Proc. IEEE Conf. Acoust., Speech Signal Process.*, May 2004, vol. 4, pp. iv-185–iv-188.

[5] S. J. Darak, V. A. Prasad, and E. M.-K. Lai, "Efficient implementation of reconfigurable warped digital filters with variable low-pass, high-pass, bandpass, and bandstop responses," *IEEE Trans Very Large Scale Integrat. Syst.*, vol. 21, no. 6, pp. 1165–1169, Jun. 2013.

[6] U. Zlzer, *DAFX - Digital Audio Effects*. New York, NY, USA: Wiley, 2011.

[7] C. Y. Yang, W. S. Chou, K. C. Chang, C. W. Liu, T. S. Chi, and S. J. Jou, "Spatial-cue-based multi-band binaural noise reduction for hearing aids," in *Proc. IEEE Workshop Signal Process. Syst.*, 2013, pp. 278–283.

[8] J. Blauert, *Spatial Hearing*. Cambridge, MA, USA: The MIT Press, 1997.

[9] *Specification for Octave-Band and Fractional-Octave-Band Analog and Digital Filters*, ANSI Standard S1.11-2004, 2004.

[10] D. Byrne, H. Dillon, T. Ching, R. Katsch, and G. Keidser, "Nal-nl1 procedure for fitting nonlinear hearing aids: Characteristics and comparisons with other procedures," *J. Amer. Acad. Audiology*, vol. 12, no. 1, pp. 37–54, 2001.

[11] Y. H. Lai, T. C. Liu, P. C. Li, W. T. Shih, and S. T. Young, "Development and preliminary verification of a mandarin-based hearing-aid fitting strategy," *PLoS One*, vol. 8, 2013, Art. no. e80831.

[12] M. A. Stone and B. C. J. Moore, "Tolerable hearing-aid delays: I. estimation of limits imposed by the auditory path alone using simulated hearing losses," *Ear Hearing*, vol. 20, no. 3, pp. 182–192, 1999.

[13] M. A. Stone and B. C. J. Moore, "Tolerable hearing-aid delays: Ii. estimation of limits imposed during speech production," *Ear Hearing*, vol. 23, no. 4, pp. 325–338, 2002.

[14] Y. T. Kuo, T. J. Lin, Y. T. Li, and C. W. Liu, "Design and implementation of low-power ansi s1.11 filter bank for digital hearing aids," *IEEE Trans Circuits Syst. I*, vol. 57, no. 7, pp. 1684–1696, Jul. 2010.

[15] C. W. Liu, K. C. Chang, M. H. Chuang, and C. H. Lin, "10-ms 18-band quasi-ansi s1.11 1/3-octave filter bank for digital hearing aids," *IEEE Trans. Circuits Syst. I*, vol. 60, no. 3, pp. 638–649, Mar. 2013.

[16] R. Brennan and T. Schneider, "A flexible filterbank structure for extensive signal manipulations in digital hearing aids," in *Proc. IEEE Int. Sym. Circuits Syst.*, 1998, vol. 6, pp. 569–572.

[17] Y. Wei and Y. Lian, "A 16-band nonuniform fir digital filterbank for hearing aid," in *Proc. IEEE Bio. Circuits Syst. Conf.*, 2006, pp. 186–189.

[18] C. Y. Yang, C. W. Liu, and S. J. Jou, "An efficient 18-band quasi-ansi 1/3-octave filter bank using re-sampling method for digital hearing aids," in *Proc. IEEE Conf. Acoust., Speech, Signal Process.*, May 2014, pp. 2639–2643.

[19] R. Bregovic, Y. J. Yu, T. Saramaki, and Y. C. Lim, "Implementation of linear-phase fir filters for a rational sampling-rate conversion utilizing the coefficient symmetry," *IEEE Trans. Circuits Syst. I*, vol. 58, no. 3, pp. 548–561, Mar. 2011.

[20] P. C. Loizou, *Speech Enhancement: Theory and Practice*. San Diego, CA, USA: Plural Publishing, 2008.

[21] R. W. Schafer and A. V. Oppenheim, *Discrete-Time Signal Processing*. Englewood Cliffs, NJ, USA: Prentice-Hall, 2009.

[22] P. P. Vaidyanathan, *Multirate Systems And Filter Banks*. Upper Saddle River, NJ, USA: Pearson Education, 2005.

[23] A. Eghbali, T. Saramaki, and H. Johansson, "On two-stage Nyquist pulse shaping filters," *IEEE Trans. Signal Process.*, vol. 60, no. 1, pp. 483–488, Jan. 2012.

[24] The MathWorks Inc. MATLAB documentation: Find minimum of constrained nonlinear multivariable function. (2015). [Online] Available:http://www.mathworks.com/help/optim/ug/fmincon.html

[25] L. Ciletti and G. A. Flamme, "Prevalence of hearing impairment by gender and audiometric configuration: Results from the national health and nutrition examination survey (1999–2004) and the keokuk county rural health study (1994–1998)," *J. Amer. Acad. Audiology*, vol. 19, pp. 672–685, 2008.

[26] Y. H. Lai, P. C. Li, K. S. Tsai, W. C. Chu, and S. T. Young, "Measuring the long-term SNRs of static and adaptive compression amplification techniques for speech in noise," *J. Amer. Acad. Audiology*, vol. 24, pp. 671–683, 2013.

[27] M. A. Stone and B. C. J. Moore, "Tolerable hearing-aid delays: Iv. effects on subjective disturbance during speech production by hearing-impaired subjects," *Ear Hearing*, vol. 26, no. 2, pp. 225–235, 2005.

[28] Y. C. Huang, Y. FanChiang, and S. J. Jou, "A pitch based vad adopting quasi-ansi 1/3 octave filter bank with 11.3 ms latency for monosyllable hearing aids," in *Proc. IEEE Workshop Signal Process. Syst.*, 2013, pp. 48–53.

Cheng-Yen Yang received the B.S. and M.S. degrees in electrical engineering from National Sun-Yat Sun University, Kaohsiung, Taiwan, in 2008 and 2010, respectively. He is currently working toward the Ph.D. degree in electronics engineering from National Chiao Tung University, Hsinchu, Taiwan. His research includes signal processing in hearing aids and related VLSI signal processing.

Chih-Wei Liu (M'03) was born in Taiwan. He received the B.S. and Ph.D. degrees, both in electrical engineering, from National Tsing Hua University, Hsinchu, Taiwan, in 1991 and 1999, respectively. From 1999 to 2000, he was an Integrated Circuits Design Engineer at the Electronics Research and Service Organization, Industrial Technology Research Institute (ITRI), Hsinchu, Taiwan. Then, near the end of 2000, he began working for the SoC Technology Center, ITRI as a Project Leader and eventually left ITRI at the end of September 2003. He is currently with the Department of Electronics Engineering and the Institute of Electronics, National Chiao Tung University, Hsinchu, Taiwan, as a Professor. His current research interests include SoC and VLSI system design, processors for embedded computing systems, digital signal processing, digital communications, and coding theory.

Shyh-Jye Jou received the B.S. degree in electrical engineering from National Cheng Kung University, Tainan, Taiwan, in 1982, and the M.S. and Ph.D. degrees in electronics from National Chiao Tung University, Hsinchu, Taiwan, in 1984 and 1988, respectively.

He joined the Department of Electrical Engineering, National Central University, Chung-Li, Taiwan, from 1990 to 2004 and became a Professor in 1997. Since 2004, he has been a Professor in the Department of Electronics Engineering, National Chiao Tung University and served as the Chairman from 2006 to 2009. Since August 2011, he has served as the Vice President, Office of International Affairs, National Chiao Tung University. He was a Visiting Research Professor in the Coordinated Science Laboratory, University of Illinois, Urbana-Champaign, during the 1993–1994 and 2010 academic years. In the summer of 2001, he was a Visiting Research Consultant in the Communication Circuits and Systems Research Laboratory, Agere Systems, Allentown, PA, USA. He received the Outstanding Engineering Professor Award, Chinese Institute of Engineers and Chinese Institute of Electrical Engineering in 2011 and 2013, respectively. He is an active contributor in IEEE, particularly the CAS Society. He served as the 2006 Chapter Chair of IEEE Circuits and Systems Society Taipei Chapter, 2009–2010 Distinguished Lecturer of the CAS Society, Guest Editor, IEEE JOURNAL OF SOLID STATE CIRCUITS, November 2008, and was Track Chair, 2011–2013 Nanoelectronics and Gigascale Systems and Technical Committee Member of VLSI Systems and Applications. He also serves as Conference Chairs, TPC Chairs in many IEEE conferences such as the Conference Chair of IEEE International Symposium on VLSI Design, Automation and Test (VLSI-DAT) and International Workshop on Memory Technology, Design, and Testing. He also served as Technical Program Chair or Co-Chair in IEEE VLSI-DAT, International IEEE Asian Solid-State Circuit Conference, and IEEE Biomedical Circuits and Systems. He has published more than 100 IEEE journal and conference papers. His research interests include design and analysis of high-speed, low-power mixed-signal integrated circuits, communication and bio-electronics integrated circuits and systems.